




Crystal and electronic structure of Co_3O_4 spinel under pressure probed by XANES and Raman spectroscopy

Emin Mijit ^{1,2,*} Kai Chen ^{3,*} João Elias F. S. Rodrigues ⁴ Zhiwei Hu,⁵ Lucie Nataf,² Angela Trapananti,¹ Andrea Di Cicco,^{1,†} and Francois Baudalet^{2,‡}

¹Physics Division, School of Science and Technology, Università di Camerino Via Madonna delle Carceri 9 I-62032 Camerino (MC), Italy

²Synchrotron SOLEIL, L'Orme des Merisiers, Saint-Aubin, BP 48, 91192 Gif-sur-Yvette Cedex, France

³Helmholtz-Zentrum Berlin für Materialien und Energie, Albert-Einstein-Strasse 15, 12489, Berlin, Germany

⁴Instituto de Ciencia de Materiales de Madrid, CSIC, Cantoblanco, E-28049 Madrid, Spain

⁵Max Planck Institute for Chemical Physics of Solids, Noethnizer Strasse 40, 01187 Dresden, Germany



(Received 28 September 2020; revised 14 December 2020; accepted 22 December 2020; published 12 January 2021; corrected 4 January 2023)

Crystal and electronic structure of Co_3O_4 spinel have been investigated by x-ray absorption near edge structure (XANES) at the Co K edge up to 58.5 GPa and Raman scattering up to 65 GPa. Several transitions have been observed upon pressurization, and the original structure was recovered on decompression. Experimental and theoretical XANES and Raman data are compatible with the occurrence of a monoclinic $P2_1/c$ phase above ~ 52.7 GPa. Vibrational modes analyzed in details by Raman scattering indicate that two other subtle transitions take place above ~ 21.9 GPa (orthorhombic $Fddd$) and ~ 43.0 GPa (monoclinic $C2/m$), in agreement with the previous x-ray diffraction experiments. Our combined experimental XANES and multiple scattering calculations indicate clear evidence of a tetrahedral to octahedral coordination crossover at the Co^{2+} sites, being completed upon transition to the monoclinic $P2_1/c$ phase. The valence and spin states at two different Co sites remained unchanged at least up to the transition onset to the monoclinic $P2_1/c$ phase ruling out the possibility of charge transfer and spin crossover in the intermediate phases as proposed previously.

DOI: [10.1103/PhysRevB.103.024105](https://doi.org/10.1103/PhysRevB.103.024105)

I. INTRODUCTION

Many oxide compounds of the AB_2O_4 family crystallizes in the spinel structure with the cubic $Fd\bar{3}m$ space group [1]. In the ideal spinel structure, the tetrahedral (T_d) and octahedral (O_h) sites are occupied by divalent A and trivalent B cations, respectively. However, in the inverse spinel, the T_d sites are occupied by half of the trivalent B cations while the O_h site are equally occupied by divalent A cations and half of the trivalent B cations. The mixed valence cobalt oxide, Co_3O_4 is a normal spinel with the form $[\text{Co}^{2+}]_{T_d}[\text{Co}^{3+}]_{O_h}\text{O}_4$. As an important magnetic, p -type semiconductor, it has been widely used in catalysts, solid state sensors, solar cells, and electrochemical energy storage [2–7]. Co_3O_4 displays strong coupling between the lattice, spin, and orbital degrees of freedom. The T_d and O_h crystal fields split the $3d$ orbital of Co^{2+} and Co^{3+} cations into $e_g^4 t_{2g}^3$ [high spin (HS), $S = 3/2$] and $t_{2g}^6 e_g^0$ [low spin (LS), $S = 0$] configurations, respectively [8]. Therefore the Co^{3+} cations at the O_h sites are diamagnetic and the magnetism of Co_3O_4 in the normal spinel structure is from the HS Co^{2+} ions at the T_d sites, which form a collinear anti-ferromagnetic ordering at low temperature below $T_N = 40$ K [9]. Spin-liquid behavior has been observed in Co_3O_4 due to the magnetic frustration at the A -site Co^{2+} ions [10].

Knowledge about the high-pressure (HP) properties of Co_3O_4 is not extended as for other similar mixed-valence spinel oxides such as magnetite (Fe_3O_4). In recent years, several studies concerning its HP phases have been carried out with controversial claims. Bai *et al.* have reported the persistence of the cubic structure up to 42.0 GPa, with a charge transfer type normal to inverse-spinel transition at 17.7 GPa [11]. However, Hirai *et al.* observed a structural transition to a monoclinic phase (space group $P2_1/c$) around 30–46 GPa [12]. They attributed this transition to a gradual charge transfer between Co^{2+} and Co^{3+} cations. Besides, they observed a different monoclinic phase (space group $C2/m$) below 28 GPa upon pressure release. Using first-principles calculations, Kaewmaraya *et al.* excluded the occurrence of this $C2/m$ phase and claimed that a local HS to LS transition takes place at the T_d Co^{2+} site, before the onset of $Fd\bar{3}m$ to $P2_1/c$ structural transition at 35 GPa [13]. In this study as well, the cubic to monoclinic transition was attributed to the charge transfer between different Co sites [13]. Very recently, a rather complete x-ray diffraction (XRD) study up to 60 GPa was performed by F. Cova *et al.* [14], in which three subsequent structural transitions were suggested: cubic ($Fd\bar{3}m$) to orthorhombic phase ($Fddd$) at 23 GPa, to a monoclinic ($C2/m$) phase at 45 GPa, and further to another monoclinic ($P2_1/c$) at 52 GPa. They have observed the direct recovery of the initial $Fd\bar{3}m$ structure from the $P2_1/c$ phase around 35–30 GPa upon pressure release.

The complexity of high-pressure experimental and theoretical results on Co_3O_4 leave many questions open, indeed,

*These authors contributed equally to this work.

†andrea.dicicco@unicam.it

‡francois.baudalet@synchrotron-soleil.fr

suggesting that a clarification about the pressure response of the local atomic, electronic and magnetic structure at the T_d Co^{2+} site in Co_3O_4 would be beneficial for the ongoing discussion. For example, charge transfer from T_d Co^{2+} to O_h Co^{3+} sites was regarded as an important factor for the occurrence of structural phase transitions [11–13]. Moreover, a local HS to LS transition at the T_d Co^{2+} was shown as a possible reason for the disappearance of magnetic moments according to the DFT study [13]. In this context, even the pressure onset of the T_d to O_h coordination crossover of Co^{2+} is still not clearly understood [12–14]. In this work, we present a detailed study of local structural and electronic properties of Co_3O_4 under pressure using XANES and Raman spectroscopy techniques. Experimental Co K -edge XANES were interpreted with the aid of state-of-the-art full multiple-scattering calculations [15–17]. Details of the local T_d to O_h coordination crossover, possibilities of charge transfer among different Co sites, order to disorder transitions, and spin crossover were discussed. Pressure induced modifications in the lattice dynamics, and changes in the local Co sites were also probed by Raman scattering. Evolutions of the vibrational modes were systematically interpreted and assigned using nuclear site group analysis combined with virtual tetrahedral/octahedral models.

II. EXPERIMENTS AND SIMULATION

Co K -edge XANES measurements have been performed under room temperature at the optic dispersive EXAFS (ODE) beamline [18] of Synchrotron SOLEIL (France). Micrometer sized Co_3O_4 powders (99% purity from Sigma-Aldrich), together with the pressure transmitting medium silicon oil, were pressurized up to 58.5 GPa in a diamond-anvil cell. High-pressure Raman experiments were performed using 4:1 methanol-ethanol mixture as pressure medium. Raman spectra were measured in back scattering geometry using a micro-Raman setup (HORIBA iH320), at selected pressure points up to 65 GPa. A green laser emitting at 532 nm was used as the excitation source. The Raman scattering signal was collected using a 50X objective and dispersed with 1800 grooves mm^{-1} grating, and detected using a Peltier-cooled CCD detector. In both experiments, pressure was systematically measured before and after each spectrum using the standard ruby fluorescence method [19]. We have used silicon oil and 4:1 methanol-ethanol mixture as the pressure mediums because they greatly simplify sample manipulation and loading, although they are not the ideal choices for ensuring hydrostatic pressure conditions. Nevertheless, we believe that slightly nonhydrostatic conditions are of minor importance and have a limited influence in the results obtained for both experimental techniques (Raman and XANES) probing essentially local structural properties.

Theoretical XANES spectra were calculated based on the first-principles one electron full multiple scattering theory using the CONTINUUM code embedded in MXAN [15–17]. The optical potential for the phase-shift calculations included the real part of the Hedin-Lundqvist exchange potential and the resulting absorption cross-section was broadened by an energy dependent Lorentzian function. The muffin-tin approximation was applied for the shape of the potential. The MT

radii were chosen according to the Norman criterion [20] with a 10% overlap. The excited configuration of the photoabsorber was considered in order to simulate the charge relaxation around the core hole. Spherical clusters of more than 200 atoms were used for calculations at different Co sites of the relevant cubic, orthorhombic and monoclinic structures (see Ref. [21] for more details).

III. RESULTS AND DISCUSSION

A. XANES investigation

1. Experimental results

As a versatile element selective tool with the sensitivity to both crystal and electronic structure, the K -edge XANES has been proven to be a very powerful tool for precise characterization of the transition metal oxides and has been successfully applied for the studies of structural, electronic, and magnetic properties of spinel oxides under HP [22,23].

The normalized Co K -edge XANES of Co_3O_4 measured at different pressure points upon pressure increase (up to 58.5 GPa) and pressure release (down to 2.3 GPa) are shown in Fig. 1(b). In order to better visualize the spectral evolution under pressure, the corresponding first derivatives of the XANES data are also shown in Fig. 1(d). Features in the pre-edge ranges (7702–7714 eV) of the XANES and first derivative data are shown with magnifications in Figs. 1(a) and 1(c), respectively. The pre-edge (~ 7707.5 eV) and the white line (~ 7728.0 eV) peaks of the XANES spectra were labeled by α and β . The first derivative spectra at the ambient pressure contains several clear features including a maximum α' and minimum α'' in the pre-edge region, and triplet features labeled as γ , σ , and ϵ in the rising edge region (7715–7730 eV).

The Co K -edge XANES features above the absorption edge originate from the excitations from Co $1s$ core level to the empty $4p$ final states, and are related to the quantum interference of multiply scattered photoelectron waves between the absorber atom and the surrounding atomic sites. The XANES spectra are therefore sensitive to the modifications in the 3D atomic configurations around the absorbing atoms, and complementary to the XRD especially at the short and intermediate range ordering. To better clarify the origin of spectral features in Fig. 1, we compared the XANES and the first derivative spectra of Co_3O_4 with the reference spectra (measured with the same setup) of CoAl_2O_4 and ZnCo_2O_4 spinel oxides, as shown in Figs. 2(a) and 2(b). CoAl_2O_4 and ZnCo_2O_4 references are the representative compounds of HS Co^{2+} and LS Co^{3+} cations at the T_d and O_h sites of spinel structure, respectively. The absorption edge (defined here as the 0.8 of the normalized height) is highly sensitive to the valence state of $3d$ transition metals [24]. From CoAl_2O_4 and ZnCo_2O_4 , there is an ~ 2.5 eV of edge energy difference, being consistent with the increase of the valence state of Co ions from 2^+ to 3^+ [25,26]. It can be seen that, qualitatively, the XANES and first derivative spectra (especially in the rising edge range) of Co_3O_4 at ambient pressure can be regarded as the superposition of the two reference spectra of CoAl_2O_4 and ZnCo_2O_4 . For example, as can be better seen in the first derivative spectra, HS Co^{2+} at the T_d site contributes to the features γ and ϵ , while LS Co^{3+} at the O_h site contributes

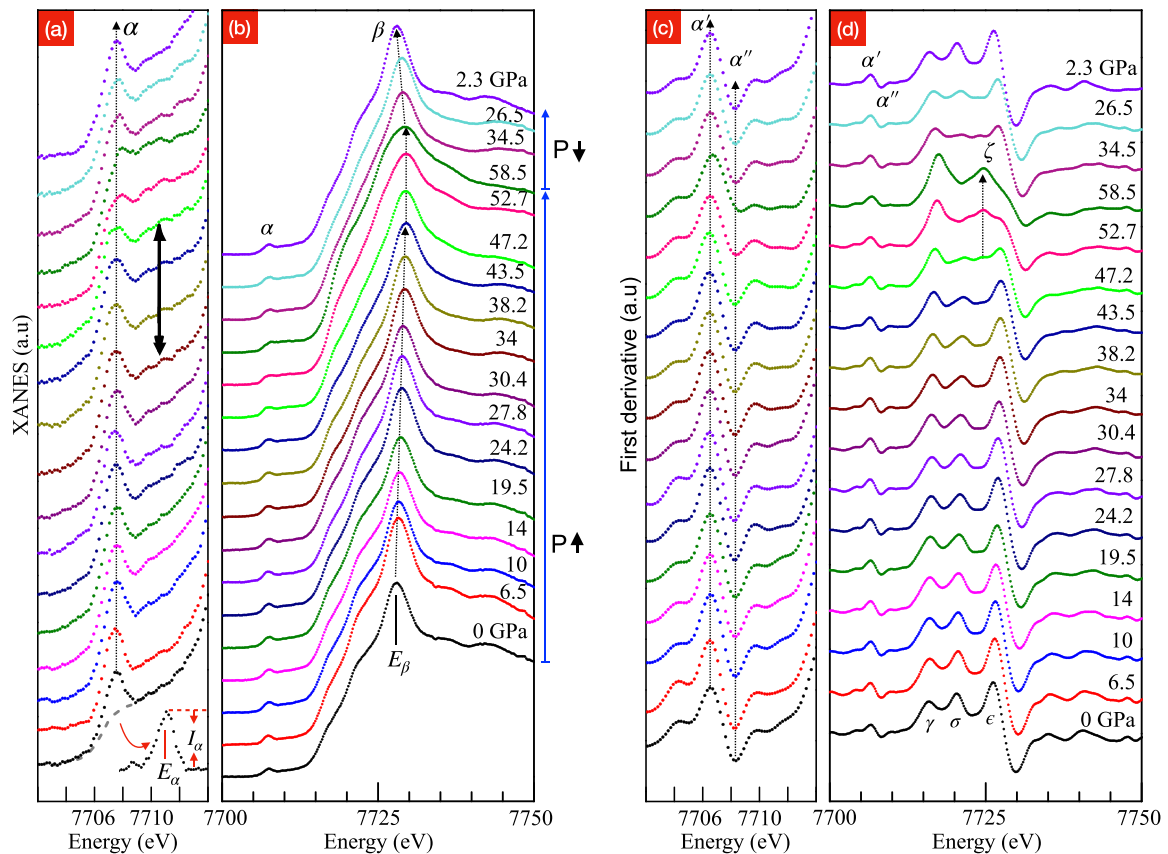


FIG. 1. XANES data (b) and their first derivative (d) upon pressure increase up to 58.5 GPa and decrease down to 2.3 GPa. For the sake of clarity, pre-edge ranges (7702–7714 eV) in XANES and first derivative spectra are shown with magnifications in (a) and (c), respectively. The intensity (I_α) and energy position (E_α) of the pre-edge peak α were defined as the peak height and peak center after removing a arctangent type background, as illustrated in the lower of part of (a).

to the peaks σ and ϵ . One can see from Fig. 2(a), that the peak α in the pre-edge range can be attributed to Co^{2+} at the tetrahedral sites, as it is observed in the spectra of both

Co_3O_4 (at 0 GPa) and CoAl_2O_4 spinels. The separate spectral contributions from T_d and O_h Co sites can be seen also from the theoretical simulations shown in Fig. S1 (Ref. [21]).

Looking back to Fig. 1, the features of the XANES and their first derivative are preserved under pressure up to ~ 43.5 GPa, but with the gradual shifts of the white line peak β [see Fig. 3(a)] and features γ , σ , and ϵ towards higher energies. Above 43.5 GPa, XANES spectral profile in Fig. 1(b) starts to show some modifications. These changes in the spectral shape can be more easily seen in the first derivative, where the feature σ gradually disappears and the feature ϵ decreases. A new broad feature which is labeled as ζ appears between feature σ and ϵ , and eventually the triplet-like profile evolves to a doublet-type feature in the 7715 ~ 7730 eV range.

Pressure dependent energy position of the white line peak β (E_β) is presented in Fig. 3(a), where it shows a change of slope in the rate of shift after 43.5 GPa. Another important detail to be noticed is the pressure response of the pre-edge feature α . Figures 3(b) and 3(c) report the intensity [I_α , defined in the inset of Fig. 1(a)] and energy position (E_α) of the peak α . As can be seen in Fig. 3(b), the intensity of α reduced slightly from 43.5 GPa, and show a clear decrease exceeding the error bars at 47.2 GPa, then finally reached to the minimum values after 52.7 GPa. While, as shown in Fig. 3(c), the energy position of α (E_α) did not shift and always kept around 7707.5 ± 0.1 eV and show a minor (~ 0.3 eV) shift starting

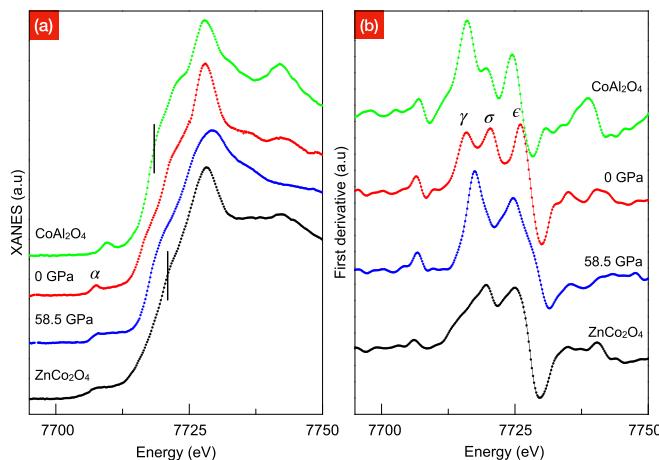


FIG. 2. XANES data (a) and their first derivative (b) at the initial (0 GPa) and final (58.5 GPa) pressures were shown together with the reference spectra of CoAl_2O_4 and ZnCo_2O_4 for comparison. Edge positions (0.8 of the edge jump) of the reference spectra were indicated by vertical bars.

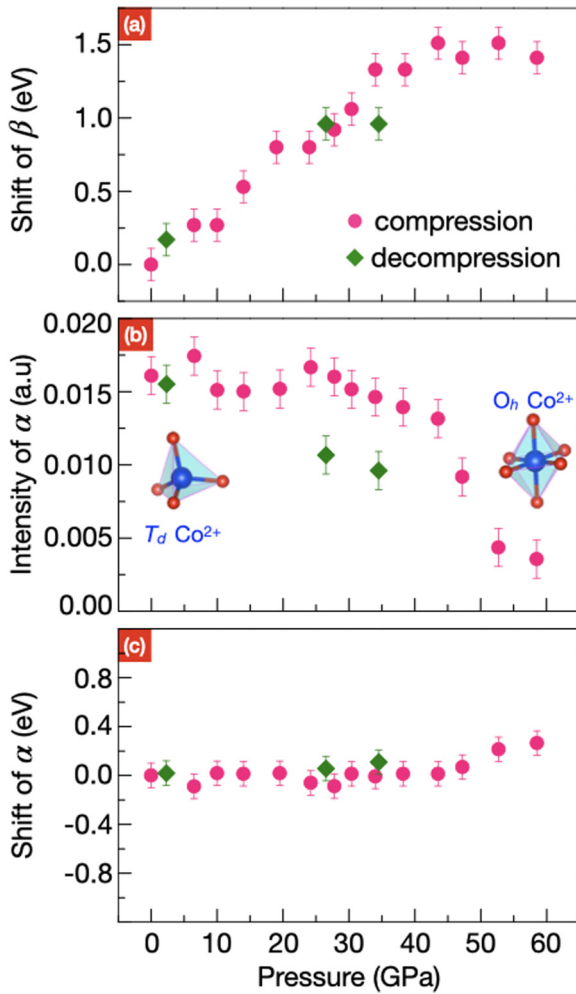


FIG. 3. (a) Pressure dependent energy shift [$E_{\beta}(P) - E_{\beta}(P = 0)$] of the white line peak β . (b) Intensity (I_{α}) of the pre-edge feature α at different pressures. (c) Pressure dependent energy shift [$E_{\alpha}(P) - E_{\alpha}(P = 0)$] of α . Purple and dark green dots represents the data points upon compression and decompression, respectively.

from 52.7 GPa. The fact of persistent energy position is the same also for features α' and α'' in the first derivative shown in Fig. 1(c). As can be more clearly observed from the features of first derivative spectra in Figs. 1(c) and 1(d), the overall characteristics of the pre-edge shape also nearly unchanged until 52.7 GPa. Above this pressure, decrease of α is reflected by the gradual flattening of the minimum feature α'' in the first derivative. The blue shift of the white line peak β and the stable energy position of the pre-edge peak α would lead to a well solved spectral feature α , instead the poorly resolved α after 47.2 GPa is indicating a change local environment of Co ion.

2. Local atomic structure

A cubic ($Fd\bar{3}m$) to orthorhombic phase ($Fddd$) transition at 23 GPa has been proposed by the recent XRD experiment [14]. In fact, the orthorhombic $Fddd$ structure was hardly identified by the XRD data and similar atomic positions and slightly different lattice constants were used for the structural refinements [14]. In order to understand the possible spectral

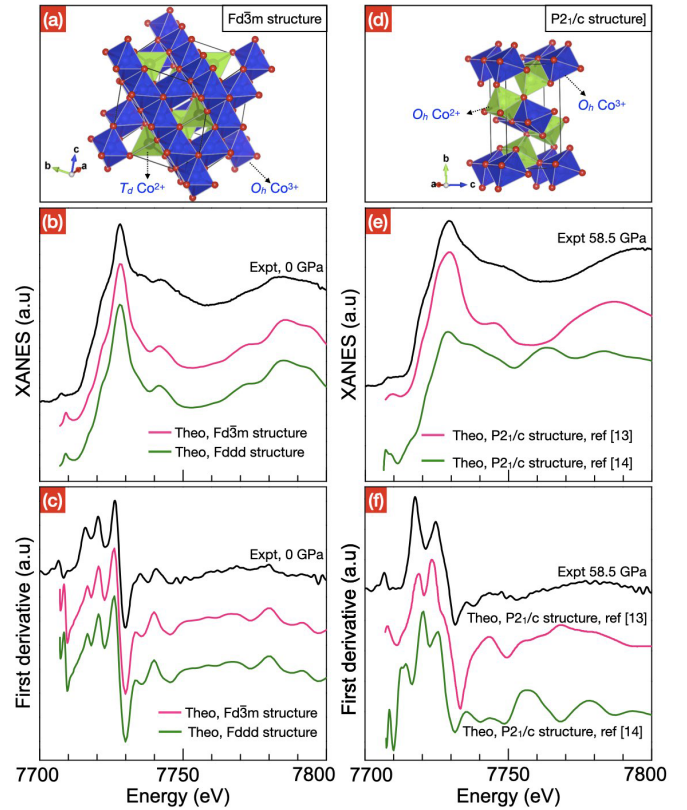


FIG. 4. (a) 3D visualization of the cubic $Fd\bar{3}m$ structure [28]. (b) Experimental XANES at 0 GPa is compared with two theoretical spectra that were calculated based on $Fd\bar{3}m$ and $Fddd$ structures which have similar atomic position in the unit cell (see Tables S1 and S2 in Ref. [21]). (c) First derivatives of the experimental and theoretical XANES given in (b). (d) 3D visualization of the monoclinic $P2_1/c$ structure [13]. (e) Experimental XANES data at 58.5 GPa is compared with the two theoretical spectra that were calculated according to the monoclinic $P2_1/c$ structures proposed in the previous studies [13,14]. (f) First derivatives of the experimental and theoretical XANES given in (e). Each theoretical spectra in (b) and (e) takes into account contributions from both Co^{2+} and Co^{3+} sites with 1:2 ratio (see Fig. S1 and other details in Ref. [21]).

modifications associated with such a subtle structural transition, we have simulated XANES spectra for both $Fd\bar{3}m$ and $Fddd$ structures using same atomic positions and slightly different lattice constant (see Tables S1 and S2 in Ref. [21]). As shown in Figs. 4(b) and 4(c), features of theoretical XANES (also their first derivatives) calculated from two structures are almost identical, and nicely reproduced the experimental spectral features at the ambient pressure. Thus it is reasonable to assume that the present XANES experiment do not identify the possible $Fddd$ phase (at 23 GPa) because of the nearly unchanged structural ordering around the Co^{2+} and Co^{3+} absorbers.

In addition to the orthorhombic $Fddd$ phase, subsequent transitions to monoclinic $C2/m$ and $P2_1/c$ phases at 45 and 52 GPa, were also observed [14]. The intermediate $C2/m$ phase co-existed with the orthorhombic structure within the 45–52 GPa range, and has been regarded as an metastable phase. Detailed structural refinement for this phase was not possible because of the overlapped diffraction peaks [14]. In

the present XANES experiment, the characteristics of spectral evolutions, such as the rate of shift (blue shift) of the white line peak β and the intensity of the pre-edge feature α starts to show clear changes at pressure above than 43.5 GPa [Figs. 3(a) and 3(b)]. Other features of the original XANES and the first derivative spectra (γ , σ , and ϵ) remain until 52.7 GPa (Fig. 1).

According to the $\Delta E \sim 1/r^2$ energy shift rule proposed by R. Natoli [27], the blue shift of the white line peak β as shown Fig. 3(a) can be interpreted as the consequence of the lattice contraction and shortening of the average Co-O bonding lengths as observed also in previous XRD experiments up to about 35 GPa [11,12]. Thus the change of slope above 43.5 GPa is correlated to the change of the Co-O contraction rate, indicating the occurrence of a phase transition and modifications in the short range ordering. The intermediate range of spectral evolution in the 43.5–52.7 GPa might be related to the metastable $C2/m$ phase that coexists with the orthorhombic phase within this pressure range. However, the lack of detailed structural information for this metastable phase hinders the possibility of spectral simulations, and thus a convincing assignment of spectral features to this metastable phase.

Completely new XANES and first derivative spectra in the 52.7–58.5 GPa range are in accordance with the transition to the $P2_1/c$ phase, which has a pressure onset at 52 GPa [14]. Detailed structural information for $P2_1/c$ phase was reported by previous theoretical and experimental studies [13,14], allowing us to simulate the corresponding XANES. In Fig. 4(e), experimental XANES at 58.5 GPa was compared with two theoretical spectra which were calculated based on those available monoclinic $P2_1/c$ structures. Corresponding experimental and theoretical first derivative spectra are shown in Fig. 4(f). As it can be seen in Figs. 4(e) and 4(f), the calculated spectrum based on the experimental $P2_1/c$ structure with highly distorted Co^{2+} sites [14], strongly disagree with the experimental XANES, while the simulated spectrum from the monoclinic $P2_1/c$ proposed by the DFT study in Ref. [13] has better qualitative agreements with the present experiment. Thus, we assign the XANES in the 52.7–58.5 range to the monoclinic $P2_1/c$ phase, with a local structure more closer (compare to the experimental one) to the one proposed by the theoretical study in Ref. [13].

The pre-edge features in the $3d$ transition metal K edges originate from $1s-3d$ quadrupole transitions or dipole like transitions due to the hybridized $3d/4p$ states, depending on the site symmetry [29]. These final states are mostly empty or partially filled bound states below the continuum, therefore pre-edge peaks usually do not shift with external pressure, being different from continuum features such as the main peak β . The intensity of the pre-edge peak is particularly sensitive to the degree of local symmetry. When the center inversion symmetry of the transition metal is broken as a result of progressive distortion from O_h to the T_d geometry, the pre-edge feature gains additional intensity due to the local $3d-4p$ orbital mixing, effectively allowing the dipole transitions to the $4p$ character of the $3d$ band [29]. Besides, the energy position of the pre-edge peak is also related to the oxidation states. In general, energy position of the pre-edge peak shifts linearly to higher energies with an increase in the valence state of the metal ions [30–35]. Because of the direct relation with the $3d$

orbital occupation, pre-edge features are also sensitive to the spin states. In particular, significant differences in pre-edge features have been observed for the different valence and spin states of Co cations at the O_h sites [36–42], while a large chemical shift of 2.7 eV has been observed from the Co^{2+} to Co^{3+} valence increase at the T_d site [43]. The changes of the Co K -edge pre-edge features were widely used for monitoring the spin and valence state transitions induced by pressure or temperature in various cobalt compounds. [38–42].

At the ambient pressure, the clear pre-edge peak α at ~ 7707.5 eV can be assigned to the Co^{2+} considering its T_d local symmetry. This was also evidenced above by comparing with the reference spectrum of CoAl_2O_4 in Fig. 2(a). The intensity of the pre-edge from LS Co^{3+} cations at the O_h sites is relatively weak and berried by Co^{2+} excitations according to a recent resonant inelastic x-ray scattering (RIXS) study [44]. This is true also when we look at the pre-edge feature of ZnCo_2O_4 reference. One can see that the LS Co^{3+} in O_h local symmetry presents a relatively weak step-like feature in the pre-edge region. Therefore intensity of the pre-edge peak is mainly dominated by the T_d Co^{2+} .

As shown in Fig. 3(b), the intensity of the pre-edge peak exhibits a clear decrease at 47.2 GPa (exceeding error bars), reaches the minimum starting from 52.7 GPa and becomes a step-like feature. As discussed above [see also Fig. 2(a)], the steplike flat pre-edge range at the highest pressure point is typical for O_h local symmetry. This indicates an increase in symmetry and T_d to O_h crossover around Co^{2+} . The pressure onset for T_d to O_h transition was remained unclear in the previous XRD studies due to the difficulties with structural refinements caused by the mixture of phases [12,14]. The behavior of the pre-edge intensity in the present experiment clearly indicates that the increase of the coordination number starts around 47.2 GPa in the vicinity of the transition pressure to the monoclinic phase, and the full O_h symmetry is reached only after the complete transition to the $P2_1/c$ phase, after 52.7 GPa. The previously reported volume collapse (densification) around this pressure (in Ref. [14]) is compatible with the possible significant increase in the atomic packing efficiency after the coordination crossover.

3. Local electronic structure

The almost unchanged energy position (E_α) of the pre-edge peak α , before it vanishes at the transition onset (52.7 GPa) to the monoclinic phase, indicates that the valence state of Co at the T_d site remains always Co^{2+} at least up to this onset pressure. This rules out the occurrence of charge transfer upon normal to inverse spinel transition that was suggested in Ref. [11]. If there would be a transition from an order to disorder system, a clear energy shift in the position of the pre-edge peak α would be expected due to the Co^{2+} to Co^{3+} valence transition at the T_d site. For such a case, 2.7 eV of chemical shift has been reported in Ref. [43]. Note that the T_d coordination of Co^{3+} is quite rare [45], and when found, the T_d $\text{Co}^{3+} - \text{O}$ bond lengths are found to be significantly short compare to their T_d $\text{Co}^{2+} - \text{O}$ counter parts [46–48]. In case of occurrence of charge transfer between two different cations sites, even with a partly Co^{2+} to Co^{3+} transition, an increase of effective valence of T_d Co^{2+} to a noninteger value is expected, and consequently a clear shift of pre-edge peak α

would be observed. As we have discussed above, the spectral features at the ambient pressure are contributed from both tetrahedral HS Co^{2+} and octahedral LS Co^{3+} [see also Fig. S1(a) in Ref. [21]]. Thus, on the other hand, the unchanged spectral profile of the XANES (including the pre-edge range) until 47.2 GPa also indicates the preserved valence and electronic configuration of T_d and O_h Co cations in Co_3O_4 before the transition onset to the monoclinic phase.

T. Kaewmaraya *et al.* have suggested the occurrence of a local HS to LS transition at the T_d Co^{2+} site before the onset of $Fd\bar{3}m$ to $P2_1/c$ phase transition [13]. This proposed magnetic transition was assumed to be correlated to the cubic ($Fd\bar{3}m$) to orthorhombic ($Fddd$) phase transition [14]. The HS to LS transition was often observed with decreasing temperature or with increase of pressure [39,41,49]. Here, occurrence of spin state transition at the T_d Co^{2+} can be excluded for two reasons. First, as discussed above, the pre-edge peak of the Co is very sensitive to the spin state of Co ions [38–42], since HS to LS transition leads to 3d hole transfer from t_{2g} to e_g orbitals, causing a transfer in the spectral weight [38–42]. Such a spin state transition is not experimentally observed in our data. Secondly, the crystal field splitting for the Co^{2+} with T_d symmetry is $10Dq(T_d) = -4/9 10Dq(O_h)$, therefore, is too weak to stabilize LS state, and LS configuration is usually not a ground state for Co^{2+} at T_d coordination [45]. For HS Co^{2+} with O_h symmetry in CoO, a HS to LS transition was observed above 90 GPa [50]. An increase of crystal field by a factor of 9/4 under pressure impossible. Furthermore, one would also expect a simultaneous collapse of lattice volume with HS to LS transition [51,52], but that was not the case until the transition to the monoclinic phases [14]. Referencing the pressure onset (90 GPa) of HS to LS transition in CoO [50], we speculate that Co^{2+} in Co_3O_4 may preserve HS state even after the complete T_d to O_h crossover at 52 GPa, and HS to LS cross might happen at much higher pressures beyond the pressure range of the present XANES experiment. Spin transition at the O_h site also can be excluded since Co^{3+} at O_h already has the LS state, pressure would further stabilize the LS state. Therefore evidences in the present XANES experiments rule out the possibility of both charge transfer and spin crossover in Co_3O_4 , at least before the transition onset (52 GPa) to the monoclinic phase.

Upon pressure release, all of the new features in the XANES and their first derivative at the highest pressure (58.5 GPa) remained until 34.5 GPa. The original spectral features at the ambient pressure, including the spectral profile, pre-edge shape and intensity starts to recover after further pressure decrease down to 26.5 GPa. Thus the occurrence of any new phase (as suggested by Ref. [12]) upon pressure release can be excluded in the present XANES experiment. It can be suggested that the original crystal structure, electronic and spin states of Co_3O_4 are fully recovered upon pressure release.

B. Raman spectroscopy study

1. Experimental results

Raman scattering is also a very sensitive probe of the local environment of metal ions in materials. Using Raman spectroscopy technique, one may access information on local

disorder [53], symmetry lowering [54], onset of phase transition [55], spin and electron phonon couplings [56–58], among other physical properties which are all dependent on the local atomic arrangements. In this work, Raman spectroscopy was employed to corroborate the results depicted by XANES technique above.

In order to probe the evolution of the lattice dynamics and successive phase transition under HP, Raman spectroscopy data were collected at selected pressures up to 65 GPa, as reported in Figs. 5(a) and 5(b). As a whole, the mode position undergoes blue shift with the increase of pressure as a result of lattice volume decrease. One may also notice a progressive increase in the phonon width as pressure increases, which is expected due to the strain and particle size effects induced under HP. The peak distribution, however, starts to exhibit substantial changes for pressures higher than 43 GPa. This is more critical around 53.7 GPa, in which new peaks can be noticed in the wave number region 700–925 cm^{-1} .

In order to better evaluate the structural phase transitions of Co_3O_4 spinel, positions of the Raman peaks ($\tilde{\nu}$, wave number) is plotted against the pressure (P) in Figs. 5(c)–5(e). This figure clearly indicates that the material experiences successive structural modifications at 21.9, 43, and 53.7 GPa. The wave number versus pressure data are fitted with a linear function $\tilde{\nu}(P) = \tilde{\nu}_0 + \alpha P$. Table I summarizes the experimental wave number under ambient condition ($\tilde{\nu}_{\text{exp}}$), the pressure intercept ($\tilde{\nu}_0$), and the pressure coefficient ($\alpha = d\tilde{\nu}/dP$), as well as the attribution of the Raman modes. The linear fittings were performed in three pressure intervals: (i) 0.1–21.9, (ii) 21.9–43, and (iii) 53.7–65 GPa. It is possible to observe an increase in the number of Raman modes fitted through an increase of pressure, which indicates a reduction in the crystal symmetry in view of the successive phase transitions. Apparently, results of the present Raman spectroscopy data are in accordance with the recent structural studies of F. Cova *et al.* [14]. Complementary to the prior research, and to our above XANES investigations, careful analysis of the present good quality Raman data allowed us to clearly identify the vibrational modes and pressure domains of various HP phases. With the better understanding of the local atomic and electronic structure from the XANES data, and clear identification of the Raman modes of different HP phases, we are able to perform a more profound analysis for the evolutions of lattice dynamics and assignments for the vibrational modes of the various Co_3O_4 phases.

2. Evolutions of vibrational modes and local structure

Systematic analysis and assignments of the vibrational modes of different HP phases can be performed in a depth way by taking advantage of the group-theory methods. Such methods provide the selection rules of the $k \approx 0$ phonons (Γ point) within the Brillouin zone. The prediction of the phonon modes may be conducted by the nuclear site group analysis, in which the site symmetry of each atomic species should be known and the irreducible representations are calculated by a set of tables available by Rousseau *et al.* [59].

For cubic Co_3O_4 with the $Fd\bar{3}m$ (SG: O_h^7 , No. 227) space group, the atomic site distributions has Co^{2+} at 8a sites (T_d), giving the representation $\Gamma_{8a} = F_{1u} \oplus F_{2g}$. Trivalent Co^{3+} cations are located at the 16d Wyckoff sites (D_{3d}), which

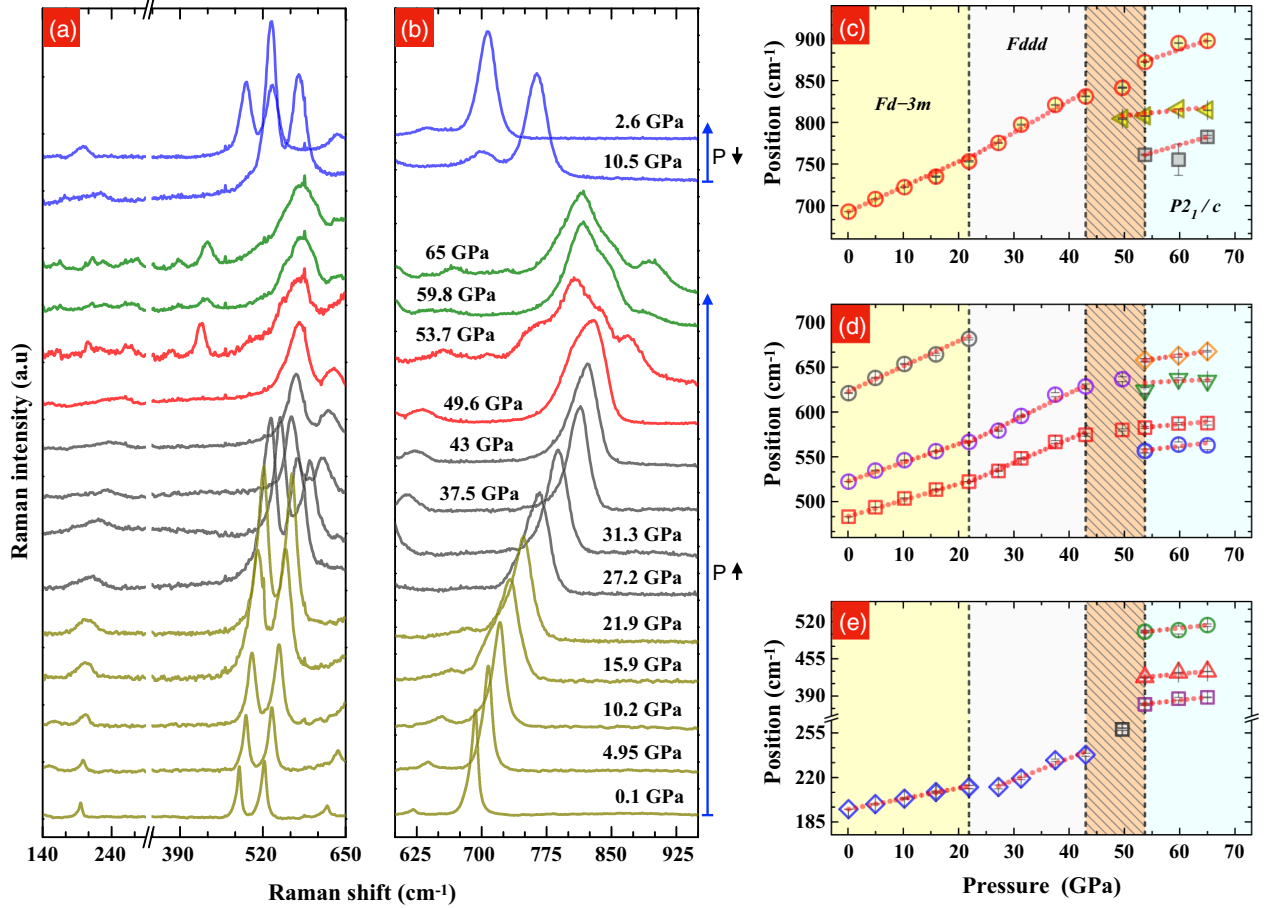


FIG. 5. [(a) and (b)] Room temperature Raman spectra under pressure from 0.1 up to 65 GPa (under compression). Raman spectra recorded upon pressure release were also given for selected pressures (10.5 and 2.6 GPa). Data are vertically shifted for clarity. The attribution of each Raman mode is available in Table I. [(c)–(e)] Pressure dependence of the experimental Raman mode wave numbers of the Co_3O_4 . The dotted lines (red) represent fits to the experimental data and the dashed vertical line corresponds to the boundary among the HP phases.

TABLE I. Experimental wave numbers of Raman modes at near atmospheric condition ($\tilde{\nu}_{\text{exp}}$), their attribution (for cubic, orthorhombic, and monoclinic phases), pressure intercept ($\tilde{\nu}_0$), and pressure coefficient ($\alpha = d\tilde{\nu}/dP$) for HP phases of Co_3O_4 spinel. For cubic and orthorhombic lattices, the internal modes (ν_1 , ν_2 , ν_3 , and ν_4) concern the vibrations of $[\text{Co}^{2+}\text{O}_4]$ tetrahedral unit, while, for monoclinic one, the internal modes (ν_1 , ν_2 , and ν_5) are Raman-active modes of $[\text{Co}^{2+}\text{O}_6]$ octahedron. T and L represent translation of Co^{3+} ion and pure libration of the molecular unit (octahedron).

$\tilde{\nu}_{\text{exp}}$ (cm^{-1})	Cubic $Fd\bar{3}m$ 0.1–21.9 GPa		Orthorhombic $Fddd$ 21.9–43 GPa			Monoclinic $P2_1/c$ 53.7–65 GPa		
	$\tilde{\nu}_0$ (cm^{-1})	α ($\text{cm}^{-1} \text{GPa}^{-1}$)	$\tilde{\nu}_0$ (cm^{-1})	α ($\text{cm}^{-1} \text{GPa}^{-1}$)	Attrib	$\tilde{\nu}_0$ (cm^{-1})	α ($\text{cm}^{-1} \text{GPa}^{-1}$)	Attrib
195.1	195.0	0.83(1)	166.5	1.7(3)	T	319.0	1.1(1)	T
						375.5	0.9(1)	L
						447.5	1.0(1)	L
						516.4	0.8(4)	L
483.2	483.4	1.82(6)	463.9	2.6(2)	ν_2	552.8	0.6(2)	ν_5
						617.6	0.3(9)	ν_5
522.4	522.8	2.08(9)	500.5	3.0(2)	ν_4	611.0	0.87(3)	ν_5
621.0	622.7	2.8(2)			ν_3	658.3	1.9(1)	ν_2
						774.2	0.7(5)	ν_2
692.8	692.6	3.0(1)	673.8	3.8(4)	ν_1	754.9	2.2(5)	ν_1

provide $\Gamma_{16d} = A_{2u} \oplus E_u \oplus 2F_{1u} \oplus F_{2u}$. As listed in Table S5 (Ref. [21]), we then expect five Raman ($A_{1g} \oplus E_g \oplus 3F_{2g}$), and four infrared ($4F_{1u}$) modes at the Γ point of the Brillouin zone. Since the Co_3O_4 spinel has well defined two sublattices: $[\text{Co}_{8a}^{2+}\text{O}_4]$ and $[\text{Co}_{16d}^{3+}\text{O}_6]$, the vibrational spectrum can be separated into external (translation and libration) and internal ($\nu_1, \nu_2, \nu_3, \nu_4$) modes assigned to the molecular unit $[\text{Co}_{8a}^{2+}\text{O}_4]$: the virtual tetrahedral model [60,61]. This unit possesses following free vibrations: Co-O symmetric (ν_1, A_1) and asymmetric (ν_3, F_2) stretchings, Co-O symmetric (ν_2, E) and asymmetric (ν_4, F_2) bendings, and also the rotational (R, F_1) and translational (T, F_2) motions as degrees of freedom [60]. Using the molecular site group analysis, the tetrahedral $[\text{Co}^{2+}\text{O}_4]$ unit can be placed into the site symmetry $8a$, while maintaining the Co^{3+} at D_{3d} sites, and the correlation among tetrahedral motions and the lattice modes of the spinel structure can be derived, as listed in Table S5 (Ref. [21]). In this way, the Raman modes are better represented by $\Gamma_R = \nu_1(A_{1g}) + \nu_2(E_g) + \nu_3(F_{2g}) + \nu_4(F_{2g}) + T(F_{2g})$.

Figures 5(a) and 5(b) illustrates details of the Raman modes of Co_3O_4 spinel with cubic lattice at the near ambient condition (~ 0.1 GPa). It is possible to detect the five expected Raman modes, being assigned as: ν_1 at 693, ν_3 at 621, ν_4 at 522, ν_2 at 483, and T at 195 cm^{-1} , corroborating previous Raman data on Co_3O_4 [62,63]. T represents the translation of the $[\text{Co}^{2+}\text{O}_4]$ group within the spinel lattice. The agreement between experimental and predicted Raman modes confirms that the Co^{2+} ions are located at T_d site symmetry at near ambient condition.

Pressure range between 23–43 GPa indicated in Figs. 5(c)–5(e) corresponds to the orthorhombic lattice with $Fddd$ (SG: D_{2h}^4 , No. 70) space group proposed in Ref. [14]. Both cubic and orthorhombic structures are quite similar, with the following atomic distribution for the orthorhombic one: Co^{2+} at 8a sites (D_2), Co^{3+} at 16d sites (C_i), and O^{2-} at 32h sites (C_1). The selection rules for the vibrational modes at the Brillouin zone-center ($k \approx 0$) can be predicted using the irreducible representation of the D_{2h} factor group [59]. Co^{2+} sites provide the representation $\Gamma_{8a} = B_{1g} \oplus B_{1u} \oplus B_{2g} \oplus B_{2u} \oplus B_{3g} \oplus B_{3u}$; The trivalent Co^{3+} sites contribute with the representation $\Gamma_{16d} = 3A_u \oplus 3B_{1u} \oplus 3B_{2u} \oplus 3B_{3u}$, while O^{2-} sites with $\Gamma_{32h} = 3A_g \oplus 3A_u \oplus 3B_{1g} \oplus 3B_{1u} \oplus 3B_{2g} \oplus 3B_{2u} \oplus 3B_{3g} \oplus 3B_{3u}$. As summarized in Table S5 (Ref. [21]), we then expect fifteen Raman ($3A_g \oplus 4B_{1g} \oplus 4B_{2g} \oplus 4B_{3g}$) modes at the Γ point. Because of the similarities between cubic and orthorhombic phases, the Co^{2+} sites also have a tetrahedral coordination and, therefore, a correlation among tetrahedral internal modes and the Co^{2+} site symmetry can be established using the correlation charts in Table S5 (Ref. [21]). The predicted Raman modes can be better understood by rewriting those fifteen phonons in terms of the vibrational modes of the $[\text{Co}^{2+}\text{O}_4]$ unit, which were placed at Wyckoff sites with D_2 symmetry:

$$\begin{aligned} \Gamma_R(Fddd) = & \nu_1(A_g) + 2\nu_2(2A_g) + 3\nu_3(B_{1g} \oplus B_{2g} \oplus B_{3g}) \\ & + 3\nu_4(B_{1g} \oplus B_{2g} \oplus B_{3g}) + 3L(B_{1g} \oplus B_{2g} \oplus B_{3g}) \\ & + 3T(B_{1g} \oplus B_{2g} \oplus B_{3g}). \end{aligned} \quad (1)$$

Therefore an enlarged number of Raman modes is expected for $Fddd$ phase; as a result of the symmetry lowering, three librational phonons ($3L$) emerged, representing rotational mo-

tions of the $[\text{Co}^{2+}\text{O}_4]$ unit. These modes usually appear in low wave-number interval ($\tilde{\nu} < 500 \text{ cm}^{-1}$) of Raman spectrum. However, by comparing the predicted modes with the experimental results shown in Fig. 5, it can be seen that the same distribution of Raman modes was maintained in the orthorhombic unit cell. This is, in turn, compatible with the fact that both cubic and orthorhombic phases are quite similar and, also, the orthorhombic distortion c/a is not so appreciable. This could hinder the splitting of degenerate E_g and F_{2g} Raman modes from the cubic lattice. Nevertheless, such a transition was manifested through the slight change in rate of peak shift.

Above 43 GPa, a new phase with a metastable character appears in coexistence with the orthorhombic one. According to the XRD experiment in Ref. [14], this metastable phase belongs to the monoclinic $C2/m$ (SG: C_{2h}^3 , No. 12); however, refinements of the atomic fractional coordinates were not possible for this $C2/m$ phase due to the overlapping of the diffraction peaks [14]. At the same time, the pressure coefficient for the observed Raman modes shows slight variations, which indicates that the metastable lattice is not too far from both orthorhombic and cubic phases and, therefore, the site symmetry of Co^{2+} is probably maintained as tetrahedrally coordinated. For pressures higher than 53.7 GPa, to a new monoclinic phase with $P2_1/c$ (SG: C_{2h}^5 , No. 14) space group starts [14]. In the $P2_1/c$, the atomic distribution is the following: Co^{2+} at 2a sites (C_i), Co^{3+} at 4e sites (C_1), and two distinct oxygens at 4e sites (C_1) [13,14]. The selection rules for the vibrational modes ($k \approx 0$) can be estimated using the irreducible representation of the C_{2h} factor group: the 2a sites provide the representation $\Gamma_{2a} = 3A_u \oplus 3B_u$, and the 4e positions contribute with $\Gamma_{4e} = 3A_g \oplus 3A_u \oplus 3B_g \oplus B_u$. We then predict eighteen Raman ($9A_g \oplus 9B_g$) modes at the Γ point.

As early discussed in the XANES analysis, for the monoclinic $P2_1/c$ phase, the coordination environment of Co^{2+} has an octahedral character (O_h), instead of the tetrahedral one observed in cubic and orthorhombic Co_3O_4 spinel. Therefore the molecular site group analysis can be performed taking into account the Raman activity of $[\text{Co}^{2+}\text{O}_6]$ unit at the 2a sites (C_i) within the $P2_1/c$ unit cell: the virtual octahedral model [64]. In this case, only the gerade modes of the free octahedron must be considered to derive the correlation among ν_1, ν_2 , and ν_5 vibrations and the lattice modes of the monoclinic structure, as summarized in correlation charts of Table S5 (Ref. [21]). Here, ν_1, ν_2 , and ν_5 denote totally symmetric stretching, antisymmetric stretching, and symmetric bending of free octahedron [65]. The predicted Raman modes can be rewritten in terms of the vibrational modes of $[\text{Co}^{2+}\text{O}_6]$ unit (which were placed at the 2a Wyckoff sites with C_i symmetry):

$$\begin{aligned} \Gamma_R(P2_1/c) = & \nu_1(A_g) + 2\nu_2(2A_g) + 3\nu_5(3B_g) \\ & + 6L(3A_g \oplus 3B_g) + 6T(3A_g \oplus 3B_g) \end{aligned} \quad (2)$$

One may notice that the number of internal modes ν_1 and ν_2 in Eqs. (1) and (2) is maintained for both $Fddd$ and $P2_1/c$ phases; the difference emerges from the three librational (L) and three translational (T) external modes in the later phase. As a result, abrupt changes (i.e., increase in the number of internal modes) in the distribution of Raman bands is not

expected for the new monoclinic phase as compared to orthorhombic one; however, it is possible to see a more rich spectral features above 625 cm^{-1} for the monoclinic lattice. It is the consequence of a more appreciable monoclinic distortion when compared to that for the orthorhombic phase. In addition, due to the variation in the site symmetry, the phonon position may change for octahedral site when compared to the tetrahedral one.

As represented in Figs. 5(c) and 5(e), it is possible to see the variation in the pressure coefficient (α) at 53.7 GPa and the occurrence of new modes in the wave-number region $390\text{--}520\text{ cm}^{-1}$, which may be attributed to three additional librational motions of $[\text{Co}^{2+}\text{O}_6]$ octahedra in the $P2_1/c$ phase. For this lattice, we also assign all the Raman modes using the virtual octahedron model, as listed in Table S5 (Ref. [21]). Again, we only detect ten modes instead of eighteen predicted as a result of possible accidental degeneracies occurring below 500 cm^{-1} . In this interval, librational, translational, and ν_5 modes may overlap their wave-number positions [64]. Figures 5(a) and 5(b) also includes selected Raman spectra collected upon pressure release (10.5 and 2.6 GPa), it is clear that the main spectral features were recovered in Co_3O_4 showing the reversibility of the phase transition.

IV. CONCLUSION

We performed an x-ray absorption and Raman spectroscopic study on Co_3O_4 spinel oxide under high pressure. Theoretical and experimental XANES spectra demonstrate the existence of a monoclinic $P2_1/c$ phase above 52.7 GPa, in accordance with the previous XRD experiment [14]. Theoretical XANES calculations suggest that the HP monoclinic phase has a similar local structure as that proposed by the DFT study [13]. XANES data suggest that the T_d to O_h local symmetry crossover at the Co^{2+} site occurs around 47 GPa, in the vicinity of the transition pressure to the monoclinic phase. The full O_h symmetry is reached only after the transition (52.7 GPa) to the monoclinic $P2_1/c$. Our results rule out the possibility of pressure induced charge transfer between T_d Co^{2+} and O_h Co^{3+} cations, thus a normal to inverse spinel

transition in Co_3O_4 is also excluded. The local HS to LS transition at the tetrahedral Co^{2+} site can not take place. We discuss that the HS to LS crossover on the Co^{2+} site may occur after the coordination increase, probably at higher pressures beyond the pressure range of the present XANES experiment.

Careful analysis of the Raman scattering data shows clear evidences of the proposed HP phases: orthorhombic $Fddd$, monoclinic $C2/m$, and $P2_1/c$ phases at 21.9, 43, and 53.7 GPa, respectively. At ambient pressure, the five modes from cubic lattice $Fd\bar{3}m$ were detected; at high pressure, the cubic-orthorhombic transition at 21.9 GPa appeared as variations in the pressure coefficient (α), while the orthorhombic/monoclinic-monoclinic at 53.7 GPa presented a first-order character in view of the occurrence of new Raman modes and changes in the pressure coefficient; this variation was also attributed to the transition from T_d to O_h like coordination around Co^{2+} ions. Vibrational modes of different Co_3O_4 phases were systematically predicted and assigned using group-theory and virtual tetrahedral/octahedral models.

Absence of spin and valence state transitions, and occurrence of T_d to O_h coordination crossover has been also suggested for the similar mixed-valence spinel oxide: Fe_3O_4 (magnetite, Fe counterpart of Co_3O_4) [23,66]. Nevertheless, results show that Co_3O_4 possesses rather unusual and complex polymorphism when compared to the magnetite and many other spinel oxides that undergo a phase transition from spinel to denser post-spinel phase with orthorhombic structures [23,67–71]. Results of the present study will enrich the general knowledge on the phase behavior of spinel oxides which are relevant in geophysics and various other fields of basic and applied science.

ACKNOWLEDGMENTS

This work has been performed within an agreement between the School of Advanced Studies of the University of Camerino and the Synchrotron SOLEIL. E. M. thanks the two institutions for supporting this research (PhD grant). J. E. thanks Carlos Pecharromán for all the support at ICMM-CSIC. All authors acknowledge Synchrotron SOLEIL for provision of beamtime.

-
- [1] X. Zhang and A. Zunger, *Adv. Funct. Mater.* **20**, 1944 (2010).
 - [2] Y. Liang, Y. Li, H. Wang, J. Zhou, J. Wang, T. Regier, and H. Dai, *Nat. Mater.* **10**, 780 (2011).
 - [3] C.-W. Tung, Y.-Y. Hsu, Y.-P. Shen, Y. Zheng, T.-S. Chan, H.-S. Sheu, Y.-C. Cheng, and H. M. Chen, *Nat. Commun.* **6**, 8106 (2015).
 - [4] M. Ando, T. Kobayashi, S. Iijima, and M. Haruta, *J. Mater. Chem.* **7**, 1779 (1997).
 - [5] L. Yan, X. Zhang, T. Ren, H. Zhang, X. Wang, and J. Suo, *Chem. Commun.* **1**, 860 (2002).
 - [6] X. W. Lou, D. Deng, J. Y. Lee, J. Feng, and L. A. Archer, *Adv. Mater.* **20**, 258 (2008).
 - [7] A. Bashir, S. Shukla, J. H. Lew, S. Shukla, A. Bruno, D. Gupta, T. Baikie, R. Patidar, Z. Akhter, A. Priyadarshi *et al.*, *Nanoscale* **10**, 2341 (2018).
 - [8] L. Suchow, *J. Chem. Ed.* **53**, 560 (1976).
 - [9] W. L. Roth, *J. Phys. Chem. Solids* **25**, 1 (1964).
 - [10] O. Zaharko, A. Cervellino, V. Tsurkan, N. B. Christensen, and A. Loidl, *Phys. Rev. B* **81**, 064416 (2010).
 - [11] L. Bai, M. Pravica, Y. Zhao, C. Park, Y. Meng, S. V. Sinogeikin, and G. Shen, *J. Phys.: Condens. Matter* **24**, 435401 (2012).
 - [12] S. Hirai and W. L. Mao, *Appl. Phys. Lett.* **102**, 041912 (2013).
 - [13] T. Kaewmaraya, W. Luo, X. Yang, P. Panigrahi, and R. Ahuja, *Phys. Chem. Chem. Phys.* **17**, 19957 (2015).
 - [14] F. Cova, M. V. Blanco, M. Hanfland, and G. Garbarino, *Phys. Rev. B* **100**, 054111 (2019).
 - [15] C. Natoli and M. Benfatto, *J. Phys. Colloques* **47**, C8-11 (1986).
 - [16] M. Benfatto, A. Congiu-Castellano, A. Daniele, and S. Della Longa, *J. Synchrotron Radiat.* **8**, 267 (2001).

- [17] K. Hayakawa, K. Hatada, S. Della Longa, P. D'Angelo, and M. Benfatto, in *X-Ray Absorption fine Structure - XAFS13: 13th International Conference*, edited by B. Hedman and P. Pianetta, AIP Conf. Proc. 882 (AIP, Melville, USA, 2007), pp. 111–113.
- [18] F. Baudalet, Q. Kong, L. Nataf, J. Cafun, A. Congeduti, A. Monza, S. Chagnot, and J. Itié, *High Pressure Res.* **31**, 136 (2011).
- [19] A. Dewaele, M. Torrent, P. Loubeyre, and M. Mezouar, *Phys. Rev. B* **78**, 104102 (2008).
- [20] J. G. Norman Jr, *Mol. Phys.* **31**, 1191 (1976).
- [21] See Supplemental Material at <http://link.aps.org/supplemental/10.1103/PhysRevB.103.024105> for the details of the theoretical XANES calculations and the nuclear site group analysis of the Raman spectroscopy data, which includes Refs. [13,14,16,28].
- [22] G. Subías, V. Cuartero, J. García, J. Blasco, S. Lafuerza, S. Pascarelli, O. Mathon, C. Strohm, K. Nagai, M. Mito *et al.*, *Phys. Rev. B* **87**, 094408 (2013).
- [23] K. Chen, F. Baudalet, Y. Mijiti, L. Nataf, A. Di Cicco, Z. Hu, S. Agrestini, A. C. Komarek, M. Sougrati, J. Haines *et al.*, *J. Phys. Chem. C* **123**, 21114 (2019).
- [24] M. Croft, D. Sills, M. Greenblatt, C. Lee, S.-W. Cheong, K. V. Ramanujachary, and D. Tran, *Phys. Rev. B* **55**, 8726 (1997).
- [25] S. Agrestini, K. Chen, C.-Y. Kuo, L. Zhao, H.-J. Lin, C.-T. Chen, A. Rogalev, P. Ohresser, T.-S. Chan, S.-C. Weng *et al.*, *Phys. Rev. B* **100**, 014443 (2019).
- [26] Z. Liu, Y. Sakai, J. Yang, W. Li, Y. Liu, X. Ye, S. Qin, J. Chen, S. Agrestini, K. Chen *et al.*, *J. Am. Chem. Soc.* **142**, 5731 (2020).
- [27] C. Natoli, in *EXAFS and Near Edge Structure III* (Springer, Berlin, 1984), pp. 38–42.
- [28] V. Brabers and A. Broemme, *J. Magn. Magn. Mater.* **104**, 405 (1992).
- [29] F. De Groot, G. Vankó, and P. Glatzel, *J. Phys.: Condens. Matter* **21**, 104207 (2009).
- [30] L. Cormier, O. Dargaud, N. Menguy, G. Henderson, M. Guignard, N. Trcera, and B. Watts, *Cryst. Growth Des.* **11**, 311 (2011).
- [31] J. Wong, F. W. Lytle, R. P. Messmer, and D. H. Maylotte, *Phys. Rev. B* **30**, 5596 (1984).
- [32] O. Villain, G. Calas, L. Gaiosy, L. Cormier, and J.-L. Hazemann, *J. Am. Ceram. Soc.* **90**, 3578 (2007).
- [33] E. Chalmin, F. Farges, and G. E. Brown, *Contrib. Mineral. Petrol.* **157**, 111 (2009).
- [34] G. Giuli, T. Eisenmann, D. Bresser, A. Trapananti, J. Asenbauer, F. Mueller, and S. Passerini, *Materials* **11**, 49 (2018).
- [35] N. C. Tomson, K. D. Williams, X. Dai, S. Sproules, S. DeBeer, T. H. Warren, and K. Wieghardt, *Chem. Sci.* **6**, 2474 (2015).
- [36] V. Cuartero, S. Lafuerza, M. Rovezzi, J. García, J. Blasco, G. Subías, and E. Jiménez, *Phys. Rev. B* **94**, 155117 (2016).
- [37] M. Giorgetti, G. Aquilanti, M. Ciabocco, and M. Berrettoni, *Phys. Chem. Chem. Phys.* **17**, 22519 (2015).
- [38] D. Mikhailova, Z. Hu, C.-Y. Kuo, S. Oswald, K. M. Mogare, S. Agrestini, J.-F. Lee, C.-W. Pao, S.-A. Chen, J.-M. Lee *et al.*, *Eur. J. Inorg. Chem.* **2017**, 587 (2017).
- [39] Y.-Y. Chin, H.-J. Lin, Z. Hu, C.-Y. Kuo, D. Mikhailova, J.-M. Lee, S.-C. Haw, S.-A. Chen, W. Schnelle, H. Ishii *et al.*, *Sci. Rep.* **7**, 3656 (2017).
- [40] J. M. Chen, J. M. Lee, S. C. Haw, S. A. Chen, V. Hardy, F. Guillou, S. W. Chen, C. Y. Kuo, C. W. Pao, J. F. Lee *et al.*, *Phys. Rev. B* **90**, 035107 (2014).
- [41] G. Vankó, J.-P. Rueff, A. Mattila, Z. Németh, and A. Shukla, *Phys. Rev. B* **73**, 024424 (2006).
- [42] J. Herrero-Martín, J. L. García-Muñoz, K. Kvashnina, E. Gallo, G. Subías, J. A. Alonso, and A. J. Barón-González, *Phys. Rev. B* **86**, 125106 (2012).
- [43] V. Cuartero, J. Blasco, G. Subías, J. García, J. A. Rodríguez-Velamazán, and C. Ritter, *Inorg. Chem.* **57**, 3360 (2018).
- [44] M. Al Samarai, M. U. Delgado-Jaime, H. Ishii, N. Hiraoka, K.-D. Tsuei, J.-P. Rueff, B. Lassale-Kaiser, B. M. Weckhuysen, and F. M. De Groot, *J. Phys. Chem. C* **120**, 24063 (2016).
- [45] N. Hollmann, Z. Hu, M. Valldor, A. Maignan, A. Tanaka, H. H. Hsieh, H.-J. Lin, C. T. Chen, and L. H. Tjeng, *Phys. Rev. B* **80**, 085111 (2009).
- [46] O. Chmaissem, H. Zheng, A. Huq, P. W. Stephens, and J. F. Mitchell, *J. Solid State Chem.* **181**, 664 (2008).
- [47] G. Muncaster, G. Sankar, C. R. A. Catlow, J. M. Thomas, S. J. Coles, and M. Hursthouse, *Chem. Mater.* **12**, 16 (2000).
- [48] A. M. Beale, G. Sankar, C. R. A. Catlow, P. A. Anderson, and T. L. Green, *Phys. Chem. Chem. Phys.* **7**, 1856 (2005).
- [49] J.-M. Chen, Y.-Y. Chin, M. Valldor, Z. Hu, J.-M. Lee, S.-C. Haw, N. Hiraoka, H. Ishii, C.-W. Pao, K.-D. Tsuei *et al.*, *J. Am. Chem. Soc.* **136**, 1514 (2014).
- [50] J. Rueff, A. Mattila, J. Badro, G. Vankó, and A. Shukla, *J. Phys.: Condens. Matter* **17**, S717 (2005).
- [51] I. Leonov, L. Pourvskii, A. Georges, and I. A. Abrikosov, *Phys. Rev. B* **94**, 155135 (2016).
- [52] Y. Sakai, J. Yang, R. Yu, H. Hojo, I. Yamada, P. Miao, S. Lee, S. Torii, T. Kamiyama, M. Lezaic *et al.*, *J. Am. Chem. Soc.* **139**, 4574 (2017).
- [53] R. L. Moreira, F. M. Matinaga, and A. Dias, *Appl. Phys. Lett.* **78**, 428 (2001).
- [54] J. Rodrigues, M. Ferrer, T. Cunha, R. Costa, J. Sambrano, A. Rodrigues, and P. Pizani, *J. Phys.: Condens. Matter* **30**, 485401 (2018).
- [55] J. Rodrigues, D. Bezerra, R. Costa, P. Pizani, and A. C. Hernandez, *J. Raman Spectrosc.* **48**, 1243 (2017).
- [56] E. Granado, J. A. Sanjurjo, C. Rettori, J. J. Neumeier, and S. B. Oseroff, *Phys. Rev. B* **62**, 11304 (2000).
- [57] J. E. Rodrigues, W. S. Rosa, M. M. Ferrer, T. R. Cunha, M. J. M. Zapata, J. R. Sambrano, J. L. Martínez, P. S. Pizani, J. A. Alonso, A. C. Hernandez *et al.*, *J. Alloys Compd.* **799**, 563 (2019).
- [58] A. Kumar, S. Chaudhary, D. K. Pandya, and S. K. Sharma, *Phys. Rev. B* **90**, 024302 (2014).
- [59] D. L. Rousseau, R. P. Bauman, and S. Porto, *J. Raman Spectrosc.* **10**, 253 (1981).
- [60] J. L. Verble, *Phys. Rev. B* **9**, 5236 (1974).
- [61] M. Silva, F. Silva, F. Sinfônio, A. Paschoal, E. Silva, and C. Paschoal, *J. Alloys Compd.* **584**, 573 (2014).
- [62] V. Hadjiev, M. Iliev, and I. Vergilov, *J. Phys. C: Solid State Physics* **21**, L199 (1988).
- [63] B. Rivas-Murias and V. Salgueiriño, *J. Raman Spectrosc.* **48**, 837 (2017).
- [64] A. Ayala, I. Guedes, E. Silva, M. Augsburg, M. del C. Viola, and J. Pedregosa, *J. Appl. Phys.* **101**, 123511 (2007).
- [65] N. N. Nath, in *Proceedings of the Indian Academy of Sciences-Section A* (Springer Nature London, UK, 1934), Vol. 1, pp. 250–259.
- [66] J.-F. Lin, J. Wu, J. Zhu, Z. Mao, A. H. Said, B. M. Leu, J. Cheng, Y. Uwatoko, C. Jin, and J. Zhou, *Sci. Rep.* **4**, 6282 (2014).

- [67] F. J. Manjon, I. Tiginyanu, and V. Ursaki, *Pressure-Induced Phase Transitions in AB₂X₄ Chalcogenide Compounds* (Springer-Verlag Berlin Heidelberg, Germany, 2014).
- [68] T. Katsura and E. Ito, *J. Geophys. Res.: Solid Earth* **94**, 15663 (1989).
- [69] T. Irifune, K. Fujino, and E. Ohtani, *Nature (London)* **349**, 409 (1991).
- [70] A. Ringwood and A. Reid, *Earth Planet. Sci. Lett.* **5**, 245 (1968).
- [71] S.-H. Shim, T. S. Duffy, and G. Shen, *Nature (London)* **411**, 571 (2001).
- Correction:* The author name Yimin Mijiti has been changed to Emin Mijit.